Geophys. J. Int. (1997) **130**, 497–505

Noise reduction and detection of weak, coherent signals through phase-weighted stacks

Martin Schimmel and Hanneke Paulssen

Department of Theoretical Geophysics, Institute of Earth Sciences, Utrecht University, PO Box 80.021, 3508 *TA Utrecht, the Netherlands.*
E-mail: schimmel@geof.ruu.nl

Accepted 1997 April 8. Received 1997 April 1; in original form 1996 August 27

SUMMARY

We present a new tool for efficient incoherent noise reduction for array data employing complex trace analysis. An amplitude-unbiased coherency measure is designed based on the instantaneous phase, which is used to weight the samples of an ordinary, linear stack. The result is called the phase-weighted stack (PWS) and is cleaned from incoherent noise. PWS thus permits detection of weak but coherent arrivals. The method presented can easily be extended to phase-weighted cross-correlations or be applied in the τ–p domain. We illustrate and discuss the advantages and disadvantages of PWS in comparison with other coherency measures and present examples. We further show that our non-linear stacking technique enables us to detect a weak lower-mantle *P*-to-*S* conversion from a depth of approximately 840 km on array data. Hints of an 840 km discontinuity have been reported; however, such a discontinuity is not yet established due to the lack of further evidence.

Key words: array, mantle discontinuities, seismic noise, time-series analysis.

INTRODUCTION AND MOTIVATION

In the determination of Earth structure, the identification of weak signals such as reflections or conversions from mantle discontinuities plays an important role. Their traveltimes, amplitudes and spatial coherencies at different frequencies are crucial for inferences about the impedance contrast, thickness and topography of the discontinuity. Identifying these weak seismic phases usually requires many good-quality seismograms and a good spatial sampling of the target. In seismic exploration the target sampling, amount of data and source can be controlled during the design of the experiment. However, in global seismology we are generally restricted due to a sparse distribution of earthquakes and stations and imprecisely known source parameters. This decreases the number of applicable techniques for signal enhancing in the usual seismological framework.

Weak phases can only be detected by their coherent appearance on different traces. Various techniques have been designed to detect coherent signals. For array data, stacking techniques can be applied where the traces are summed along assumed traveltime curves. These can be the normal-moveout (NMO) curves for reflected phases or just straight traveltime curves for slant stacks. Assuming that the summation of seismograms is performed along the correct traveltime curve, the signal is expected to sum up constructively while the surrounding noise amplitude should decrease. An important factor for the noise reduction is of course the data quality. Unfortunately, a large part of the seismogram consists of signal-generated noise. Consequently, other larger and more prominent phases in the vicinity of our weak signal are considered noise. Even though they stack less coherently than our signal they can appear as large-amplitude features in the stack and lead to ambiguous phase detection. The difficulty in suppressing noise using ordinary stacks was the motivation for non-linear stacking techniques such as the *n*th root process of Muirhead (1968) and Kanasewich, Hemmings & Alpaslan (1973). In seismology the *n*th root stack has been successfully applied in the detection of weak non-prominent phases such as *s670P* (Richards & Wicks 1990) or *s920P* (Kawakatsu & Niu 1994) conversions. Another motivation for non-linear stacking is to lower the threshold for event detection. For instance, Weichert (1975) successfully used a logarithmic process similar to the *n*th root processing. A number of other beamforming techniques exist. Neele & Snieder (1991) increased the resolution of the conventional beamforming by applying inverse theory in order to optimize the array response. Krüger *et al.* (1993) designed a double-beam method, which combines source and receiver array beamforming. Zürn & Rydelek (1994) recalled the phasor-walkout method to show how coherent harmonic signals such as the eigen modes of the Earth can be detected on single time-series. They used a graphical representation of the Fourier transform which reveals the random, coherent or periodic nature of signals in a complex spectrum. In addition, Rydelek & Sacks (1989) applied phasor walkouts to detect periodicities in earthquake catalogues. Phasor walkouts and

the method proposed here, although very different, are based on the same principle, namely the phase coherency of complex signals.

In exploration seismology a function called semblance (Taner & Koehler 1969) is widely used to detect coherent signals across an array, and semblance-weighted slant stacks are used for signal detection (e.g. Stoffa *et al.* 1981; Kong, Phinney & Roy-Chowdhury 1985). Here we present a similar technique, which is based on a more direct coherency measure by involving instantaneous phases. It is called a phase-weighted stack and we will use the abbreviation PWS. We will show an application and discuss the PWS in comparison with the nth root stack (Muirhead 1968), energy-normalized cross-correlation (Neidell & Taner 1971), the coherency functional (Gelchinsky, Landa & Shtivelman 1985) and semblance (Taner & Koehler 1969).

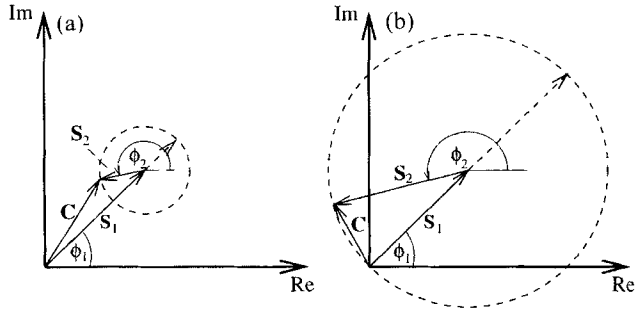

Figure 1. (a) Illustration of the summation of two samples from analytic traces $S_1(t)$ and $S_2(t)$ in the complex plane. The sum vector C is not very sensitive to changes in the instantaneous phase Φ_2. (b) $S_1(t)$ and $S_2(t)$ are normalized on a sample-by-sample basis. C is now very sensitive to changes in the instantaneous phase. $|C|$, the phase stack, is a direct measure of the coherency.

METHOD

We present a coherency measure which is explicitly independent of the amplitude and use this measure to weight the samples of the linear stack. The coherency measure is based on the instantaneous phase of the unstacked traces as will be shown using complex trace analysis. We outline the method below.

Analytic signal and phase stacks

In complex trace analysis an analytic signal or complex trace $S(t)$ is constructed from the seismic trace $s(t)$. This is done by ascribing the seismic trace $s(t)$ to the real part of the analytic signal and its Hilbert transform $H(s(t))$ to the imaginary part of $S(t)$. The analytic signal then takes the form $S(t) = s(t) + iH(s(t))$. The analytical signal can also be expressed with time-dependent amplitude $A(t)$ and phase $\Phi(t)$:

$$S(t) = s(t) + iH(s(t)) = A(t)\exp[i\Phi(t)]. \tag{1}$$

$A(t)$ is the envelope of $s(t)$ and $\Phi(t)$ is called instantaneous phase (e.g. Bracewell 1965). We visualize the analytic trace as a vector with length $A(t)$ which rotates with progressing time in the complex space around a time axis (Taner, Koehler & Sheriff 1979). The projection of this curve onto the surface spanned by the real axis and the time axis is our seismic trace $s(t)$.

We picture the linear or ordinary stack $1/N\,\Sigma\, s_j(t)$ as the real part of the sum of the analytic traces. Index J enumerates the N traces used. Fig. 1(a) schematically shows the stack of two analytic traces $C(\tau) = S_1(\tau) + S_2(\tau)$ at fixed time $t = \tau$, that is on a sample-by-sample basis. Let us assume that the phase of $S_2(\tau)$ is variable, then we know $C(\tau)$ ends on the circle indicated with dashed lines. The envelope $|C(t)|$ will be maximal if both instantaneous phases $\Phi_1(\tau)$ and $\Phi_2(\tau)$ are equal. In that case the signal is coherent. The sum of incoherent signal adds to a smaller $|C(\tau)|$. $|S_1(\tau)|$ will in general differ from $|S_2(\tau)|$, and in the presence of large-amplitude noise $|C(t)|$ can be larger for noise than for the tiny coherent signal. The stack of small data sets in particular is biased by this sort of noise. We bypass this and increase the S/N ratio for $|C(t)|$ by normalizing the analytic traces $S_1(t)$ and $S_2(t)$ sample by sample. This is illustrated in Fig. 1(b) and we call the following sum a *phase stack*, since no amplitudes are explicitly involved:

$$c(t) = \frac{1}{N}\left|\sum_{j=1}^{N}\exp[i\Phi_j(t)]\right|, \tag{2}$$

where N is the number of traces used. The amplitudes of the phase stack range between 0 and 1 as a function of time. If the instantaneous phases of the signals at a certain time are coherent, then the amplitude of the phase stack equals one. Zero amplitude means that the signals summed up completely destructively. The phase stack is a measure of coherency as a function of time, that is the effectiveness of the stack on the base of the instantaneous phase is described. The amplitudes of the seismic traces are only involved in computing the instantaneous phase. We would like to mention here that the phase stack $c(t)$ can be smoothed similarly to other measures which are mainly used in seismic exploration. Hereafter the smoothed phase stack $\widetilde{c(t)}$ is obtained by averaging over a time-gate centred at time t with width $2T$:

$$\widetilde{c(t)} = \frac{1}{2T+1}\sum_{\tau=t-T/2}^{t+T/2} c(\tau). \tag{3}$$

In eq. (3), t, τ and T are indices rather than time variables.

Phase-weighted stacks

The objective is to suppress stacked signals which are not coherent. For this purpose we involve the phase stack as a coherency measure for the sum of seismic traces. The idea is to use the phase stack as a time-dependent weight of the linear stack. This is easily performed by the multiplication of both terms:

$$g(t) = \frac{1}{N}\sum_{j=1}^{N} s_j(t)\left|\frac{1}{N}\sum_{k=1}^{N}\exp[i\Phi_k(t)]\right|^{\nu}. \tag{4}$$

Now it becomes clear why we call this a *phase-weighted stack* (PWS): every sample of the linear stack will be weighted by the coherency of its instantaneous phases. Weak coherent signals are enhanced through the incoherent noise reduction. The phase stack acts as a filter with a certain sharpness of the transition between phase similarity and dissimilarity, which is controlled by the power ν. The linear stack is retrieved with $\nu = 0$. The PWS is a non-linear stack, and waveform distortion is expected. However, coherent signals will not be distorted

too much since the instantaneous phase is presumed to be more or less stationary on the individual traces. The strongest distortions are expected for incoherent signals. In the following we involve synthetic data to show the merits of PWS and phase stack.

APPLICATION TO SYNTHETIC DATA

In subsequent sections we show the performance of PWS using synthetic data. This encompasses a qualitative comparison of PWS with the linear stack and the nth root stack (Muirhead 1968; Kanasewich *et al.* 1973), which is another effective non-linear stacking technique. A second important issue which is addressed in this section is the coherency measure itself. We compare the phase stack with other coherency measures which are often applied in seismic exploration.

Phase-weighted stack versus linear stack

In the following example we compare the abilities of the PWS and linear stack to detect coherent signals and to distinguish them from signal-generated noise. Fig. 2(a) shows 10 synthetic seismograms. Arrows with numbers label the distinct arrivals to simplify their naming. The same seismogram section but with superimposed noise is illustrated in Fig. 2(b). Note that it seems impossible to recognize all arrivals by eye due to relatively high-amplitude noise. Figs 2(c) and (d) demonstrate the squared phase stacks (PS), linear stacks (LS) and PWSs at zero slowness. The squared phase stack ($\nu = 2$) is used to calculate the PWS. It can be regarded as the power of the phase stack that helps to increase the S/N ratio. [We would like to mention here that an analytic signal with zero amplitude theoretically does not have a phase. However, numerically a phase zero is ascribed to a zero-amplitude signal. Consequently, phase stacks of zero-amplitude traces equal one. In Fig. 2(c) the phase stack deviates from one due to numerical noise in the time-series of Fig. 2(a).] The phase stack of Fig. 2(c) equals one for the coherent arrivals 1 and 4, and is still large for arrival 2, which interferes with arrival 3. The noise-contaminated data yield a phase stack (Fig. 2d) which indicates coherency for the same arrivals. Due to the noise they are less coherent than in Fig. 2(c), but stand out clearly from the surrounding noise.

Note that from Fig. 2(b) it seems to be impossible to distinguish between coherent arrival 4 and 'signal-generated noise' 5 and 6. Indeed, all three arrivals show up as a clear signal in the linear stack and thus might be misinterpreted as coherent arrivals. However, the PWSs (bottom traces in Figs 2c and d) allow the distinction to be made. They are cleaned from arrivals 5, 6 and other noise. This is justified since the

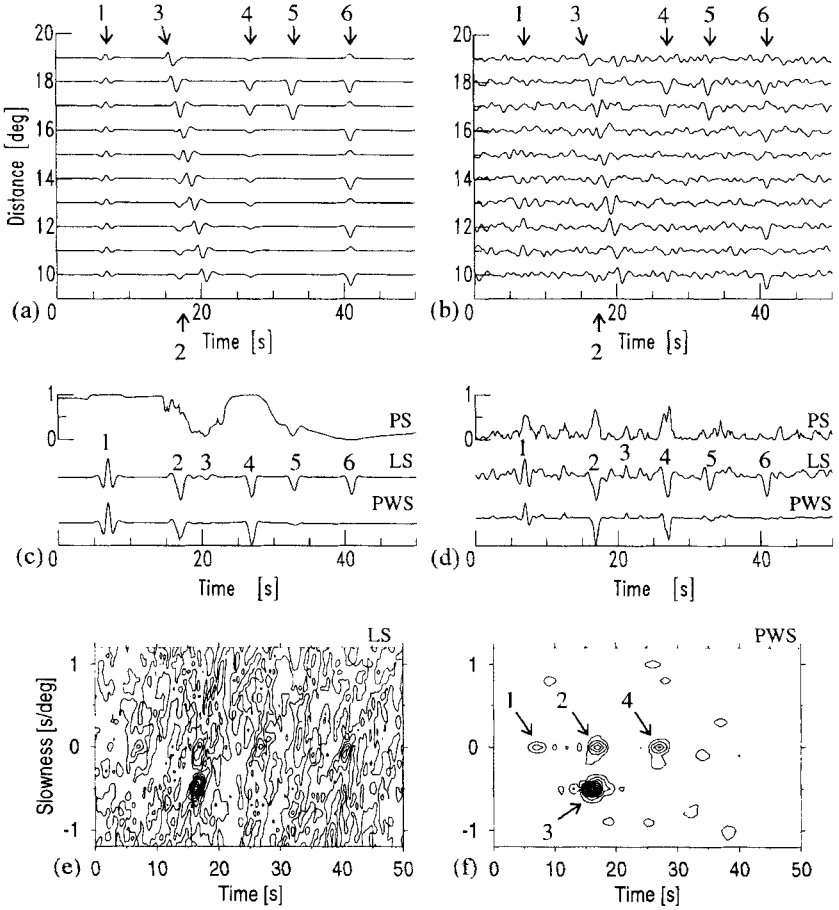

Figure 2. (a) Synthetic seismograms with different arrivals labelled by numbers. (b) Same as (a) but with random noise. (c) From top to bottom: squared phase stack, linear stack and PWS for the noise-free seismograms. (d) Same as (c) but for the seismograms with noise. (e) and (f) show normalized slant stacks of the noisy data of (b). The stacks are performed with respect to the trace at 10° over a slowness range of -1.2 to 1.2 s deg^{-1}. The envelopes of the linear stacks (e) and PWSs (f) are contoured at 0.1 intervals.

PWS is constructed from the linear stack by multiplication with the phase stack. Phases 5 and 6 are not coherent over the array (see Fig. 2a) and are therefore down-weighted by the phase stack. This decision could not have been made by inspecting the noisy data themselves or the linear stack. Note that the random noise is similarly down-weighted.

Figs 2(e) and (f) show the contoured envelopes of the linear stacks and PWSs at different slownesses. The stacks are performed with respect to the trace at a distance of 10°. Both slant stacks are normalized to 1 and contoured for intervals of 0.1. PWS enables a correct slowness and arrival-time determination of all weak arrivals, while the linear stack is too noisy. PWS is indeed cleaned from signal-generated noise that in the linear stack might lead to misinterpretations.

Phase stack versus other coherency measures

Many other coherency measures are based on the cross-correlation coefficients of real or complex traces. Some of them differ by normalization. For the subsequent comparison, three coherency measures commonly used in seismic exploration have been selected.

Fig. 3(a) shows four time-series, each with a wavelet at about 3 and 8 s. Their waveforms, arrival times and amplitudes are similar, except one wavelet at 8 s which is three times larger. Some small-amplitude noise has been added to the traces.

First we apply the energy-normalized cross-correlation sum [after eq. 10 in Neidell & Taner (1971) but for analytic traces] to our data. The first trace in Fig. 3(b) shows the result. The second trace of Fig. 3(b) shows the 'coherency functional' of Gelchinsky *et al.* (1985) (their eq. 21). This measure is normalized by the cross-correlation sum of the envelopes. Note that these two measures can reach negative values. Third, (Fig. 3b, third trace) we apply the semblance, which is defined as an output-to-input energy ratio (Taner & Koehler 1969; Neidell & Taner 1971). The output energy is determined by the squared stack, and the input energy by the stack of squared traces. The last trace in Fig. 3(b) shows the squared phase stack. Squaring has been used, since the other measures also involve the power 2. Note that the squared phase stack becomes similar to the semblance, which uses real traces and explicitly involves amplitudes. Semblance and phase stack range between 0 and 1.

In exploration seismology the coherence measurements are often smoothed by averaging over a time-gate, such as in eq. (3). The influence of a 0.4 s time-gate is illustrated by the traces in Fig. 3(c). Smoothing is a simple and often used filter used to stabilize waveforms and simplify signal detection. Throughout this paper we do not apply further smoothing, since we want to present the method in its plain form without obscuring any undesired features.

All these measures have in common the fact that they become equal to 1 in the case of phase and amplitude similarity, that is for equal instantaneous phase and envelope. This is fulfilled for the first arrival in our data in Fig. 3(a) and explains the maximum values between 3 and 5 s in Figs 3(b) and (c). Note that the semblance reaches 0 whenever the corresponding sample of the stack has zero amplitude. This causes the high-frequency character of the semblance function and justifies smoothing.

The cross-correlation sum, coherency functional and semblance are amplitude-biased coherency measures. Consequently, these measures do not depend on the waveforms alone but also on their relative amplitudes. This means that if one changes the amplitudes without modifying the waveforms then the coherence measure generally varies. The signals at ~8–10 s in our data in Fig. 3(a) have equal instantaneous phases but varying amplitudes. The cross-correlation sum and semblance give a coherency smaller than 1 (Figs 3b and c), as they penalize coherent signals with varying amplitudes. Conversely, the coherency functional and phase stack result in a coherency of 1. Both measures perform equally well for our data. The phase stack is not sensitive to varying amplitudes since no amplitude information is involved (see eq. 2). The coherency functional is amplitude-unbiased only for the phase coherency of all the records.

We want to mention that the measures applied to our data are based on different design philosophies. For instance,

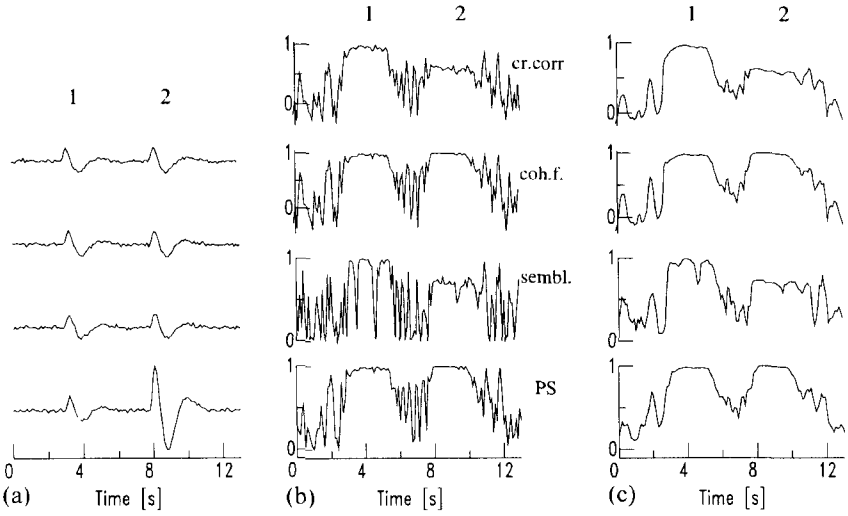

Figure 3. (a) Synthetic time-series with two arrivals each. Waveforms are all similar but the amplitude of the second signal of the last trace is multiplied by three. (b) From top to bottom: cross-correlation sum, coherency functional, semblance and phase stack for data from (a). (c) Same as (b) but smoothed with a time-gate width of 0.4 s (5 samples).

penalizing signals with varying amplitude can be advantageous for certain applications. For our application we consider the phase stack (Fig. 6d) to be the better coherency measure, since it is not biased by the signal amplitudes and thus justifies its use for weighting stacks. Especially for the detection of weak signals, we should not punish these when their amplitudes vary.

Phase-weighted stack versus *n*th root stack

Lastly we compare our stacking technique with another often used non-linear stacking technique: the so-called *n*th root stack (Muirhead 1968; Kanasewich *et al.* 1973). We treat it separately here because, due to the non-linearity, the results might appear similar to PWS. The *n*th root stack is defined as

$$y(t) = \text{sign}(r(t))|r(t)|^n, \tag{5}$$

where

$$r(t) = \frac{1}{N}\sum_{j=1}^{N} \text{sign}(s_j(t))|s_j(t)|^{1/n}. \tag{6}$$

The power n is a number larger than or equal to 1. The linear stack is retrieved with $n = 1$; $n > 1$ leads to a non-linear amplification which brings out small-amplitude signals more clearly. It occurs at the expense of waveform distortion (e.g. Kanasewich *et al.* 1973), which for simple signal detection might not be of importance. In Fig. 4 we compare the PWS (a) with the *n*th root process (b) for the data of Fig. 2(b). The uppermost panel of Fig. 4 shows the linear stacks as they are obtained by both techniques with $v = 0$ and $n = 1$, respectively. The labels mark the coherent signals. The other panels show the ability of both methods to enhance the coherent signals by increasing the power. We observe that the waveform distortion due to non-linearity is smaller in the PWS than in the *n*th root traces. The waveforms in the *n*th root traces become narrower for increasing n. This waveform distortion can even go so far that spurious arrivals seem to be generated, although in this example they are very small. We have marked them with an open circle in Fig. 4(b). A comparison with the linear stack shows that these arrivals are in fact part of one wavelet. Strong spurious arrivals can be recognized in the real data example from Fig. 7. Both PWS and *n*th root stack seem to be appropriate for signal detection. However, PWS is based on a more physical background of phase coherency and permits a separation into its components, namely the linear stack and phase stack.

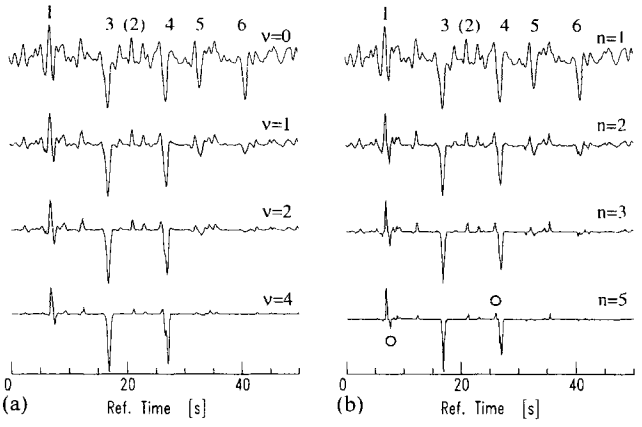

Figure 4. PWS (a) versus *n*th root stack (b) at different powers (v and n) for data from Fig. 2(b). Uppermost stacks ($v = 0$, $n = 1$) equal the linear stack. Labels 1, 2 and 4 mark the coherent arrivals. Open circles mark the onset of spurious signals which can appear to be independent arrivals.

APPLICATION TO REAL DATA

In the following we illustrate the performance of the stacking techniques and the coherency measures by using real data. We selected data from an earthquake which occurred 599 km underneath the Peru–Brazil border region (10.97°S, 70.78°W) on 1990 October 17. The nine broad-band seismograms used are recordings from the NARS-NL array [Network of Autonomously Recording Stations which was employed in The Netherlands at that time (Paulssen, Van der Lee & Nolet 1990)]. The arrivals we detect are weak and less coherent than in the synthetic case study. A qualitative comparison of the different techniques evidently points to the advantages of phase stack and PWS.

Phase stack versus linear stack

Data pre-processing consists of the rotation of the horizontal components to obtain radial and transverse polarized records, aligning the data to zero time with respect to the *P* arrival and bandpassing them between 0.02 and 0.2 Hz. The three components of every recording have been normalized with respect to the *P* phase on the *Z*-component. Fig. 5(a) shows the *P*-wave coda including the *pP* phase at about 129 s on the radial components. These traces have been summed, yielding the linear stack. Its envelope (dotted line) and phase stack (dashed line) are plotted in Fig. 5(b). From the phase stack it is obvious that there are three coherent phases (marked by a dot) in the coda of the *P* phase (excluding *pP*). However, this is not evident from the envelope of the linear stack. What is more, the signal between 80 and 90 s on the linear stack might easily be misinterpreted as a coherent arrival, whereas the phase stack shows that it is not. As a result we expect it to be down-weighted in the PWS. The squared phase stack ($v = 2$) is used to calculate the PWS. Linear stack (dotted lines) and PWS (solid lines) for the *R*- and *Z*-components are displayed in Figs 5(c) and (d). The amplitude range plotted corresponds to 12 per cent of the *P* wave amplitude on the *Z*-component. Note that the amplitudes of the PWS are smaller than or equal to the amplitudes of the linear stack since the coherency weight does not become larger than 1.

The first two arrivals marked with a filled circle in Fig. 5(b) can be identified as *S* waves which left the source as *P* waves, since there is no coherent arrival on the *Z*-component and since they arrive too early for a pure *S* wave. The first dot marks a *Psms* phase which reverberated once in the crust as an *S* wave. Its amplitude on the PWS trace is about 60 per cent of the linear stacked amplitude. Thus the *Psms* phase experienced a 40 per cent amplitude reduction due to incoherencies. The first multiple reverberation *Psms2* (*Psmssms*) also appears in the linear stack (open circle in Fig. 5c), but is obviously much more incoherent since it is much more strongly down-weighted in the PWS than the *Psms* arrival. The second dot in Fig. 5(b) marks a *P* phase converted to *S* at the 410 km discontinuity (*P410s*). The linear stack shows the *P410s* phase and the first Moho multiple *Psms2* with similar amplitudes. However, in the PWS *P410s* stands out more clearly since it

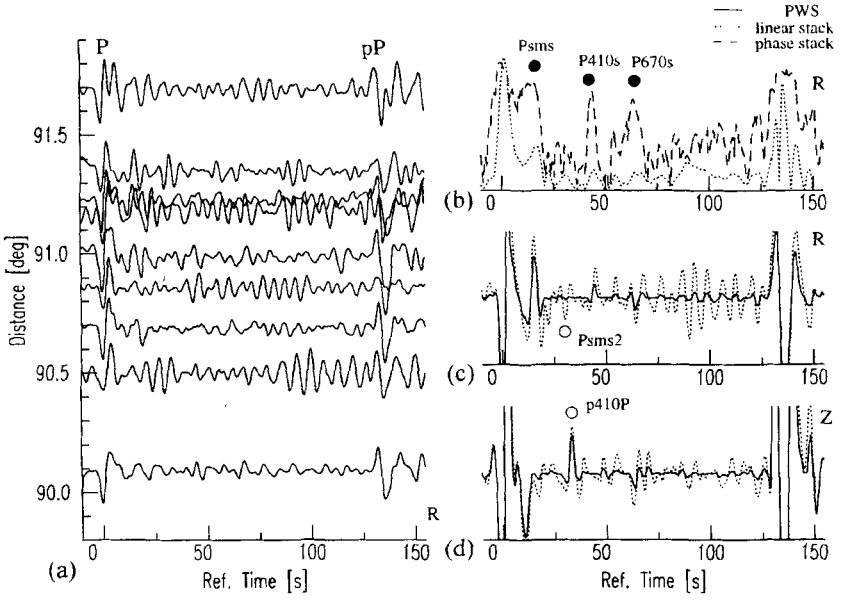

Figure 5. (a) Radial traces recorded at NARS-NL, aligned with respect to the *P* phase on the *Z*-component and bandpassed between 0.02 and 0.2 Hz. (b) Envelope of the linear stack (dotted line) and phase stack (dashed line) for data presented in (a). (c) Linear stack (dotted line) and PWS (solid line) for the *R*-component. Maximum amplitude plotted corresponds to 12 per cent of the *P*-wave amplitude on the *Z* component. (d) Same as (c) but for the *Z*-component.

sums up more coherently. The interpretation of the third signal in Fig. 5(b) is more ambiguous since there is also energy on the *Z*-component (Fig. 5d). Phase-weighted slant stacking showed that there is interference of two arrivals at about 66 s which are separated by more than 1 s deg^{-1} in the slowness domain. One (*P670s*) has predominant energy on the radial component, the other at larger slowness has more energy on the vertical component. Finally, the open circle in Fig. 5(d) indicates a clear longitudinally polarized arrival. It could be a *P*-wave reverberation near the source or receiver. A possible explanation would be a *p410P* phase, which is a near-source underside reflection from the 410 km discontinuity. This signal is almost not down-weighted, and is thus very coherent.

Fig. 5 shows that the detection of the coherent signal is simplified due to the amplitude reduction of the incoherent signal. The amplitude reduction cleaned the PWS from the incoherent signal, and together with the linear stack permits a more unambiguous phase detection.

Phase stack versus other coherency measures

Here we apply the energy-normalized cross-correlation sum (Fig. 6a), coherency functional (6b), semblance (6c) and squared phase stack (6d) to the data of Fig. 5(a).

Fig. 6 enables a direct qualitative comparison between the abilities of the different techniques to detect weak phases. For instance, Figs 6(a)–(c) show many large-amplitude signals. However, some of these (marked by an open circle) do not coincide with the picks of Fig. 6(c). From the phase stack we know that the coherency increases with the similarity of instantaneous phases only. This is its essential advantage, since it enables one to detect weak arrivals that are more coherent than the surrounding signal. The coherency measures of Figs 6(a)–(c) depend on the amplitudes. This dependence can obscure or feign weak coherent arrivals by assigning a coherency which is smaller than the coherency of a less phase coherent but larger-amplitude arrival.

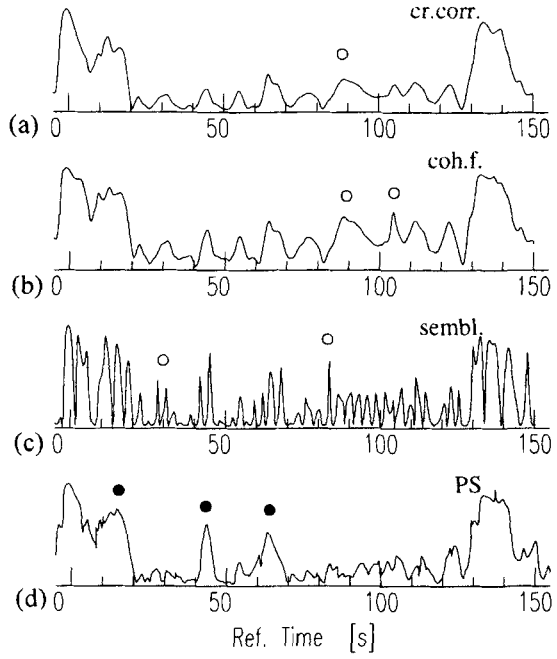

Figure 6. Energy-normalized cross-correlation sum (a), coherency functional (b), semblance (c) and squared phase stack (d) for data from Fig. 5(a).

Among Figs 6(a)–(c) the semblance (Fig. 6c) seems to give the best coherency measure. However, a larger variation in amplitude of the coherent arrivals would result in a much poorer semblance (see Fig. 3). We want to recall that this

measure is usually smoothed. However, smoothing would not improve the S/N ratio.

Phase-weighted stack versus *n*th root stack

We now apply the *n*th root stack (Muirhead 1968; Kanasewich *et al.* 1973) to the data of Fig. 5(a). In Fig. 7 PWS (a) is compared with the *n*th root process (b). The uppermost panel of Fig. 7 shows the linear stacks as they are obtained by both techniques with $v = 0$ and $n = 1$, respectively. The other traces show that both methods efficiently suppress noise. We observe that the waveform distortion is smaller in the PWS than in the *n*th root traces, as spurious arrivals (open circles) seem to be generated by this last method. Comparison with the linear stack shows that these arrivals are in fact part of one wavelet. Note that such artefacts are well known and might be recognized in, for instance, Kanasewich *et al.* (1973) and Richards & Wicks (1990).

Although PWS and the *n*th root stack perform almost equally well on our data, we prefer to apply PWS for the detection of weak but coherent signals. PWS seems to suffer less from waveform distortions and spurious phases, which can be larger than the coherent signal. It further permits a separation into the linear stack and its phase coherency, the phase stack.

ANOTHER APPLICATION: DETECTION OF WEAK *P840s* PHASES

Lastly we illustrate how PWS helped us to detect a coherent weak phase which is not predicted by standard earth models. We selected data from three more events, with hypocentres beneath Northwest Argentina (1991 June 23, 26.8°S 63.35°W, 558 km, $m_b = 6.4$), the Bonin Island region (1991 May 3, 28.08°N 139.59°E, 433 km, $m_b = 6$) and Peru (1991 July 6, 13.11°S 72.19°W, 105 km, $m_b = 6.2$). The events were recorded at 9, 4 and 5 broad-band receivers of the NARS-NL array, respectively. Data were processed similarly to the recordings from the Peru–Brazil event. Fig. 8 shows the linear stacks (a,c) and the PWSs (b,d) of the radial (solid lines) and vertical components (dotted lines) of the Argentina and Bonin Island events. The Argentina event (Figs 8a and b) has an epicentral distance of $\sim 100°$ to the reference station used for data alignment. Consequently, the first arrival is a core-diffracted *P* wave. The epicentral distance of the Bonin Island earthquake is 90°. The first arrivals are the *P* and *PcP* phases. The clear observation of radially polarized signals 80 s after the first arrivals is striking. They are marked with filled circles in the

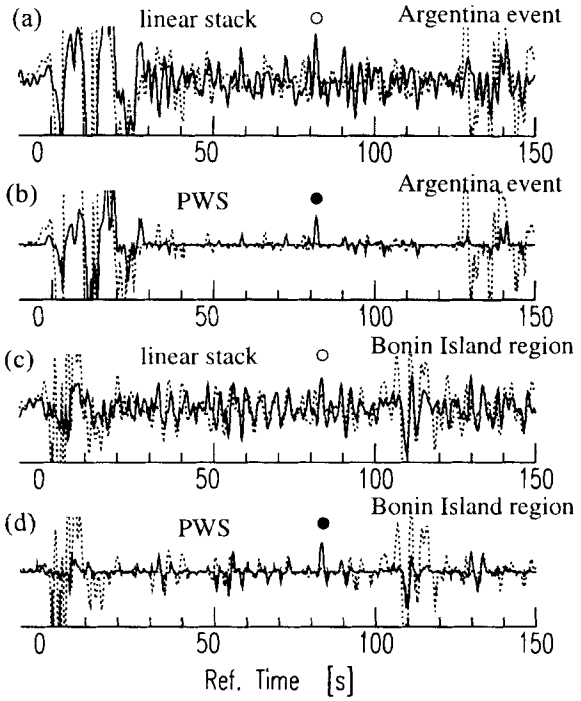

Figure 8. Linear stack for the Argentina event (a) and the Bonin Island event (c). (b) and (d) contain the corresponding PWSs. The *Z*- and *R*-components are shown with dotted and solid lines, respectively. The data are bandpassed between 0.05 and 0.6 Hz. Filled circles point to the clear *P840s* arrival in the PWS, while open circles mark the same phase in the linear stack.

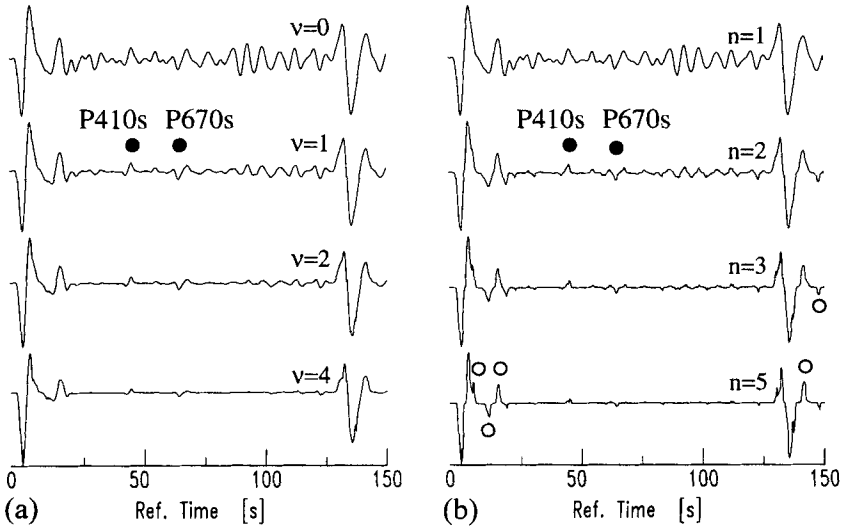

Figure 7. PWS (a) versus *n*th root stack (b) at different powers (v and n) for data from Fig. 5(a). Uppermost stacks ($v = 0$, $n = 1$) equal the linear stack. Open circles mark spurious signals which appear to be independent arrivals.

PWSs in Figs 8(b) and (d). After recognizing them on the PWSs, they are also identified on the linear stacks, where they are marked with open circles. This phase is also present in the stacks of the Peru–Brazil event (from Fig. 5, at higher frequencies, however) and for the Peru event.

The interpretation could be either a *P*-to-*S* conversion from a discontinuity at a depth of approximately 840 km (*P840s*) or a *Pp220s* phase which experiences one surface reflection and a reflection conversion at 220 km depth. Both phases arrive at about the same time and are indistinguishable by slowness, using the NARS-NL data per event. Possible *Pp220s* phases were observed for the North American craton by Bostock (1996). However, comparing the differential traveltime from the Argentina event and the Peru or Peru–Brazil event (these three events have almost the same backazimuths), one finds a negative differential slowness, as is predicted for the *P840s* phase. There are two other points in favour of a *P840s* rather than a *Pp220s* phase. (1) A *Pp220s* phase experiences one more reflection and two extra passages through the uppermost mantle than a *P840s* phase would do. We therefore do not expect that a *Pp220s* phase is coherent at high frequencies, as will be shown below. (2) A *Pp220s* phase has multiplicity 5, which means there are four other phases with the same traveltime and slowness. These are *Ps220p*, *p220sP*, *P220sp220p* and *p220ps220P*. One would expect a hint of these phases on the PWS of the vertical component. Altogether, we favour *P840s* over *Pp220s*.

In Fig. 9 we manually aligned the stacked P_{diff} and *P* phases on the *Z*-components (dashed lines) and the *P840s* phases on the *R*-components (solid lines) to obtain the best waveform coherency between both phases. To achieve this the vertical traces had to be multiplied by −1 and shifted by 79 s (9a) and 79.5 s (9b and c), respectively. The coherency between both phases at high frequencies is striking. This means that little waveform distortion occurred at the high frequencies, and a sharp 840 km discontinuity can be inferred (Richards 1972; Paulssen 1988). For instance, a 4 km thick linear transition zone at about 840 km depth yields a transmission coefficient which decreases at 1 Hz to about 80 per cent and at 1.5 Hz to about 60 per cent of the transmission coefficient at zero frequency. Increasing the transition zone would increase the frequency dependence and waveform distortion. Note that the polarity of the *P840s* phase is opposite to that of the first arrival. This would imply a small *S*-velocity decrease at about 840 km. First evidence for *P840s* phases was presented by Paulssen (1988). She performed linear stacks of 48 events with different azimuths (mainly from the Japan region), recorded at individual NARS stations, and illustrated a clear signal on the radial component. Shearer (1990) reported observing a hint of a *Pp840p* phase in his global data stacks. Such a phase has a multiplicity two; this means it can be a near-source or near-receiver reflection. In a 1-D earth, both arrive at the same time and sum to double amplitude. Poupinet (1974) required a strong *S*-velocity gradient at 850 km depth in order to model a *PL(S)* coupled wave observed at 40° epicentral distance. There is no global evidence for an 840 km discontinuity and we do not have any additional information to explain its nature. Its study is not the purpose of this paper.

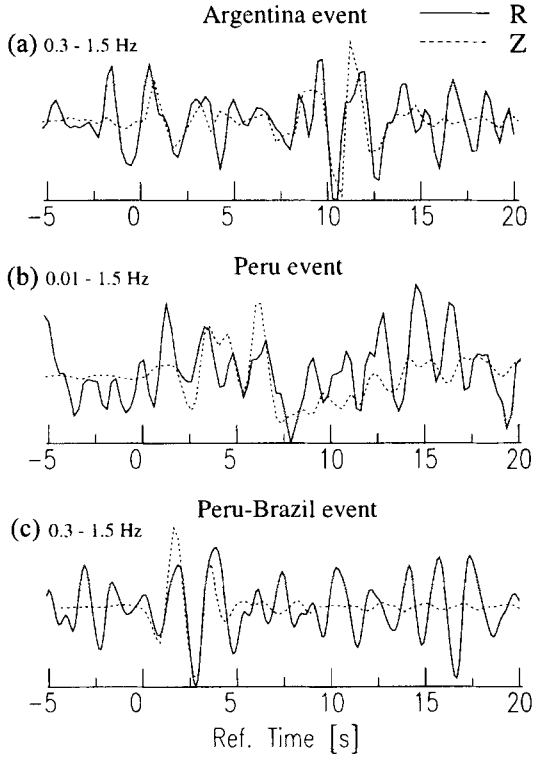

Figure 9. Stacked waveforms with P_{diff} (a) and *P* (b and c) on the *Z*-components (dashed lines) and *P840s* on the *R*-components (solid lines). Dashed traces are normalized, multiplied by −1, and shifted by 79 s (a) and 79.5 s (b and c).

DISCUSSION AND CONCLUSIONS

We have developed a non-linear stacking technique for enhancing signals through incoherent noise reduction. The results are stacked traces which are cleaned from incoherent noise. This enables the detection of weak signals, even for a small amount of data.

Similar to PWS, phase-weighted cross-correlations can be designed and used for signal recognition or arrival-time picking. The phase stack can further be used to weight the misfit function between synthetic and stacked waveform data. Its advantage would be that one avoids fitting large-amplitude noise better than weak but coherent portions of the waveform. In this paper we restricted ourselves to PWS and illustrated its applicability. No quantitative investigation of the merits of PWS was performed, but the examples presented justify its use for the detection of weak phases. For instance, the *P*-to-*S* conversions in Figs 5, 8 and 9 were not detectable in the linear stacks, but they were in the PWSs.

The advantages compared to other non-linear stacking techniques are two-fold. (1) The phase-weighted stack can be separated into a phase stack and a linear stack. This enables a better control of the physics behind the non-linear process. The phase stack is an amplitude-unbiased coherency measure. (2) Waveform distortion of coherent signals is expected to be minimal since these signals should be stationary in phase over the entire waveform. Consequently, waveform distortion does not depend on amplitudes but on the coherency of the components of the stack. Due to the coherency weight, the stack is more sensitive to time offsets and therefore allows a more accurate slowness determination. In other words, phase-weighted slant stacks can improve the time and slowness resolution of weak and coherent phases.

In this paper we found evidence for a discontinuity at about 840 km. This discontinuity is detected from events with different azimuths and seems to be sharp at least locally beneath the Netherlands. More observations and a more detailed study of the 840 km discontinuity are required to explain its nature.

ACKNOWLEDGMENTS

We would like to thank Axel Röhm and Roel Snieder for stimulating us to publish this work. The comments of an anonymous reviewer, Gunnar Jahnke and Michael Weber are appreciated. The NARS network is supported by the Earth Sciences branch of the Netherlands Organization for Scientific Research (GOA). This is Geodynamic Research Institute (Utrecht University) publication 96.044.

REFERENCES

Bostock, M.G., 1996. A seismic image of the upper mantle beneath the North American craton, *Geophys. Res. Lett.*, **23,** 1593–1596.

Bracewell, R.N., 1965. The Fourier transform and its applications, Mcgraw-Hill, New York, NY.

Gelchinsky, B., Landa, E. & Shtivelman, V., 1985. Algorithms of phase and group correlation, *Geophysics,* **50,** 596–608.

Kanasewich, E.R., Hemmings, C.D. & Alpaslan, T., 1973. N-th root stack nonlinear multichannel filter, *Geophysics,* **38,** 327–338.

Kawakatsu, H. & Niu, F., 1994. Seismic evidence for a 920-km discontinuity in the mantle, *Nature,* **371,** 301–305.

Kong, S.M., Phinney, R.A. & Roy-Chowdhury, K., 1985. A nonlinear signal detector for enhancement of noisy seismic record sections, *Geophysics,* **50,** 539–550.

Krüger, F., Weber, M., Scherbaum, F. & Schlittenhardt, J., 1993. Double beam analysis of anomalies in the core-mantle boundary region, *Geophys. Res. Lett.*, **20,** 1475–1478.

Muirhead, K.J., 1968. Eliminating false alarms when detecting seismic events automatically, *Nature,* **217,** 533–534.

Neele, F. & Snieder, R., 1991. Are long-period body wave coda caused by lateral inhomogeneity?, *Geophys. J. Int.*, **107,** 131–153.

Neidell, N.S. & Taner, M.T., 1971. Semblance and other coherency measures for multichannel data, *Geophysics,* **36,** 482–497.

Paulssen, H., 1988. Evidence for a sharp 670-km discontinuity as inferred from *P* to *S* converted waves, *J. geophys. Res.*, **93,** 10 489–10 500.

Paulssen, H., Van der Lee, S. & Nolet, G., 1990. The NARS-Netherlands Project, *IRIS Newsletter,* **9** (4), 1–3.

Poupinet, G., 1974. *PL(S)* a 40° et la discontinuité de vitesse de *S* à 850 km de profondeur, *Ann. Géophys.*, **30,** 127–139.

Richards, M.A. & Wicks, C.W., 1990. *S–P* conversions from the transition zone beneath Tonga and the nature of the 670 km discontinuity, *Geophys. J. Int.*, **101,** 1–35.

Richards, P.G., 1972. Seismic waves reflected from velocity gradient anomalies within the earth upper mantle, *Z. Geophys.*, **38,** 517–527.

Rydelek, P.A. & Sacks, I.S., 1989. Testing the completeness of earthquake catalogues and the hypothesis of self-similarity, *Nature,* **337,** 251–253.

Shearer, P.M., 1990. Seismic imaging of upper-mantle structure with new evidence for a 520-km discontinuity, *Nature,* **344,** 121–126.

Stoffa, P.L., Buhl, P., Diebold, J.B. & Wenzel, F., 1981. Direct mapping of seismic data to the domain of intercept time and ray parameter—A plane-wave decomposition, *Geophysics,* **46,** 255–267.

Taner, M.T. & Koehler, F., 1969. Velocity spectra-digital derivation and applications of velocity functions, *Geophysics,* **84,** 859–881.

Taner, M.T., Koehler, F. & Sheriff, R.E., 1979. Complex seismic trace analysis, *Geophys.*, **44,** 1041–1063.

Weichert, D.H., 1975. Reduced falsed alarm rates in seismic array detection by non-linear beamforming, *Geophys. Res. Lett.*, **2,** 121–123.

Zürn, W. & Rydelek, P.A., 1994. Revisiting the phasor-walkout method for detailed investigation of harmonic signals in time series, *Surv. Geophys,* **15,** 409–431.